J. Appl. Comput. Mech., 7(3) (2021) 1334-1347
DOI: 10.22055/JACM.2019.27729.1432

ISSN: 2383-4536
jacm.scu.ac.ir

Shahid Chamran University of Ahvaz

Journal of Applied and Computational Mechanics

Research Paper

# Non-similar Solutions of MHD Mixed Convection over an Exponentially Stretching Surface: Influence of Non-uniform Heat Source or Sink

**P.M. Patil[1], D.N. Latha[1], A.J. Chamkha[2]**

[1] Department of Mathematics, Karnatak University, Pavate Nagar, Dharwad – 580003, India, Email: pmpatil@kud.ac.in
[2] Faculty of Engineering, Kuwait College of Science and Technology, Doha, Kuwait

Received November 29 2018; Revised February 16 2019; Accepted for publication February 19 2019.
Corresponding author: A.J. Chamkha (a.chamkha@kcst.edu.kw)


**Abstract.** In this paper, an analysis of magnetohydrodynamic (MHD) mixed convection over an exponentially stretching surface in the presence of a non-uniform heat source/sink and suction/injection is presented. The governing boundary layer equations are transformed into a set of non-dimensional equations by using a group of non-similar transformations. The resulting highly non-linear coupled partial differential equations are solved by using the implicit finite difference method in combination with the quasilinearization technique. Numerical results for the velocity, temperature and concentration profiles, as well as the skin friction coefficient, wall heat transfer and mass transfer rates are computed and presented graphically for various parameters. The results indicate that the velocity profile reduces, while the temperature profile increases in presence of the effects of magnetic field and suction at the wall. The velocity ratio parameter increases the skin-friction coefficient and the Schmidt number decreases the wall mass transfer rate. The temperature profile increases for the positive values of Eckert number and space as well as temperature dependent heat source/sink parameters, while the opposite behavior is observed for negative values of same parameters.

**Keywords:** Magnetohydrodynamics (MHD); Mixed convection; Exponentially stretching sheet; Non-uniform heat source/sink; Suction/injection.

## 1. Introduction

Magnetohydrodynamics (MHD) is a field of study that combines elements of electromagnetism and fluid mechanics to describe the flow of electrically conducting fluids. MHD couples Maxwell's equations of electromagnetism with hydrodynamics to describe the macroscopic behaviors of conducting fluids such as plasmas. MHD flow plays a vital role in solar physics, astrophysics, heat and mass transfer, planetary magnetospheres, chemical engineering, and many industrial and agricultural applications. Alfven [1] pioneered the study of MHD, for which he received the 1970 Nobel Prize in physics. Due to its valuable applications in various areas of science, considerable progress has been made in the study of heat and mass transfer in MHD flows. In recent years, Ahmed *et al.* [2] have examined the analytical solutions of a MHD mixed convection flow of an incompressible, viscous Newtonian fluid by using the perturbation method. Rauf *et al.* [3] dealt with the laminar steady three-dimensional mixed convective magnetohydrodynamic boundary layer of a Casson nanofluid over a bidirectional stretching surface. Hayat *et al.* [4] examined the influence of melting heat transfer in the stagnation point flow of an incompressible magnetohydrodynamic (MHD) tangent hyperbolic fluid. Hayat *et al* [5] dealt with the magnetohydrodynamic (MHD) three-dimensional flow of second grade nanofluid in the presence of convective boundary condition. Hayat *et al* [6] studied the stagnation point flow of MHD Carreau fluid with

Published online: November 19 2019

heterogeneous–homogeneous reactions. Further, many researchers [7-20] have contributed vital results pertaining to the technique of magnetohydrodynamics.

During the last few decades, due to its useful applications in several industrial manufacturing processes such as the extraction of plastic sheets, hot rolling, and the cooling of metallic plates in a cooling bath, the problems of heat transfer in the boundary layer of a continuous stretching surface have attracted many researchers. Hossam and Hassan [21] dealt with the boundary layer flow and heat transfer of an electrically conducting viscous fluid over a stretching sheet. Magyari and Keller [22] analyzed heat and mass transfer in the boundary layer on an exponentially stretching continuous surface. Bidin and Nazar [23] studied a numerical solution of the boundary layer flow over an exponentially stretching surface with thermal radiation. Mukhopadhyay [24] explained slip effects on MHD boundary layer flows over an exponentially stretching sheet with suction/blowing and thermal radiation. Jusoh *et al.* [25] have considered the magnetohydrodynamic rotating flow and heat transfer of a ferrofluid due to an exponentially permeable stretching/ shrinking sheet.

In recent studies, especially in physical problems, non-uniform heat source/ sink effects on heat transfer have grabbed the attention of investigators, due to their numerous applications. Pal and Chatterjee [26 – 27] and Rahman *et al.* [28] have included the effects of a non-uniform heat source, but considered only viscous fluid. Bhukta et al. [29] carried out research on non-uniform heat source/ sink and dissipation effects on MHD mixed-convection flow over a stretching surface in a porous medium. Mabood and Ibrahim [30] presented a numerical analysis of the effects of Soret and non-uniform heat source on MHD non-Darcian flow over a stretching sheet. Mabood *et al.* [31] investigated the effects of non-uniform heat sources on the two-dimensional MHD mixed-convection heat and mass transfer flow of a micropolar fluid over a stretching sheet through a non-Darcian porous medium. Mahantesh *et al.* [32] analyzed the effects of a non-uniform heat source/ sink on MHD viscoelastic boundary layer flow over an impermeable stretching sheet. Ramesh *et al.* [33] analyzed MHD mixed convection flow of a viscoelastic fluid over an inclined surface with a non-uniform heat source/ sink.

The effects of suction and injection along a stretching surface for mixed convection have attracted many investigators, due to the double impacts projected with respect to heat transfer. Ramesh *et al.* [34] investigated the MHD flow of dusty fluid near the stagnation point over a permeable stretching sheet with the effect of a non-uniform source/ sink. Sandeep and Sulochana [35] examined the effects of a non-uniform heat source/ sink, mass transfer, suction/ injection, and chemical reaction on MHD unsteady mixed-convection boundary layer flow of a micropolar fluid over a stretching/ shrinking surface. Chamkha [36] investigated the Soret and chemical reaction effects on mixed-convection MHD flow past a vertical plate with suction over a porous medium in the presence of heat absorption.

In the present research paper, the non-similar transformations [37-38] are utilized to get the dimensionless partial differential equations from the dimensional one. In case of non-similarity approach, the solution profiles have $x$-dependency, i.e. profiles shape varies along the length of the stretching sheet. However, for similarity case, the solution profiles do not have $x$-dependency and the profiles have same shape along the length of the stretching sheet. Therefore, the non-similarity case represents a real world problem. Also, the techniques of magnetohydrodynamics and non-uniform heat source/sink assist for the cooling processes in various industries. Thus, the present problem analyzes the heat and mass transfer of mixed convection flow over an exponentially stretching surface with non-similarity approach and this study can assist the designers in various industrial sectors.

The paramount interest of this study is to investigate the influence of non-uniform heat source/ sink effects due to mixed convection on MHD flow over a semi-infinite vertical permeable exponentially stretching sheet with the effects of suction/ injection. The governing equations are transformed into a set of nonlinear coupled partial differential equations, which is then solved by the finite difference method in combination with the quasilinearization technique [39-40]. The variations in the velocity, temperature and species concentration profiles are studied for various values of the physical parameters. Also, the effects of the skin friction coefficient, rate of heat, and mass transfer at the surface are studied in detail. The investigation carried out in this research paper may be useful for the design engineers in the polymer industries, where the stretching of the polymer and molding it into required shapes needs cooling processes. In such cases, the techniques of magnetohydrodynamics and non-uniform heat source/sink can be utilized, appropriately.

## 2. Formulation of the Problem

We consider the laminar steady flow of an incompressible electrically conducting viscous fluid over an exponentially stretching sheet. The physical model and coordinate system are considered as shown in Fig. 1. The $x$- and $y$-axes are taken in the direction along and perpendicular to the fluid motion, respectively. Furthermore, a transverse magnetic field $B_0$ is applied normal to the flow field. The temperature and species concentration at the surface are maintained uniform at the values $T_w$ and $C_w$, respectively, which are different from the ambient temperature $T_\infty$ and species concentration $C_\infty$. A temperature-dependent non-uniform heat source/sink and suction/injection are imposed on the permeable exponentially stretching plate which is considered in the current investigation. All thermo-physical properties of the fluid in the flow model are assumed to be constant, except in density variation causing the body force in momentum equation. The Boussinesq approximation is invoked for the energy to relate the density changes and to couple in this way the temperature field to the flow field [41].

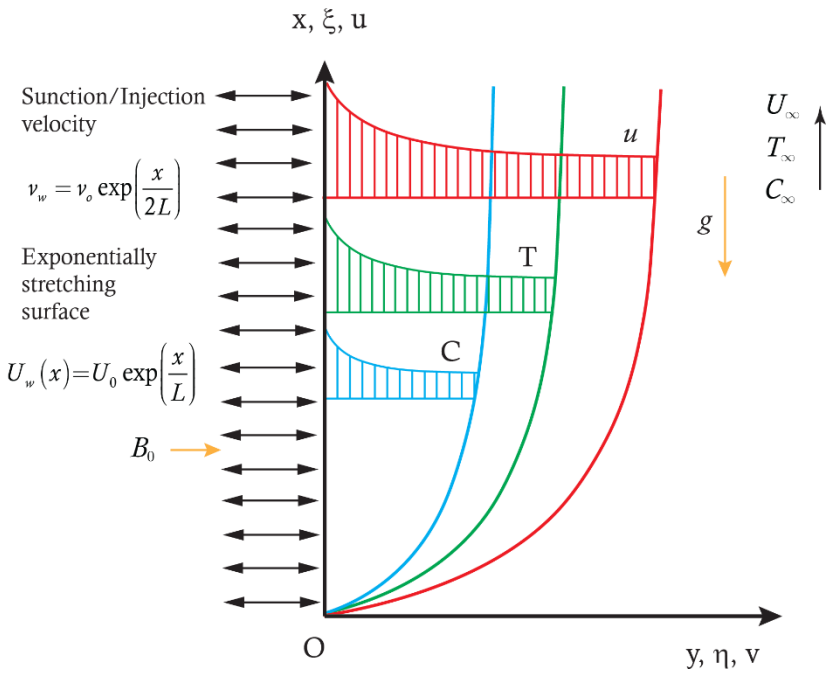


**Fig. 1.** Physical model and coordinate system.

Under these assumptions, the boundary layer equations governing the flow, heat and mass transfer take the form, with the usual notations, as [42 - 43]:

$$\frac{\partial u}{\partial x} + \frac{\partial v}{\partial y} = 0 \tag{1}$$

$$u\frac{\partial u}{\partial x} + v\frac{\partial u}{\partial y} = \nu\frac{\partial^2 u}{\partial y^2} + \frac{\sigma B_0^2}{\rho}(U_e - u) + g\left[\beta(T - T_\infty) + \beta^*(C - C_\infty)\right] \tag{2}$$

$$u\frac{\partial T}{\partial x} + v\frac{\partial T}{\partial y} = \frac{\nu}{\Pr}\frac{\partial^2 T}{\partial y^2} + \frac{q'''}{\rho C_p} + \frac{\sigma B_0^2}{\rho C_p}(U_e - u)^2 \tag{3}$$

$$u\frac{\partial C}{\partial x} + v\frac{\partial C}{\partial y} = \frac{\nu}{Sc}\frac{\partial^2 C}{\partial y^2} \tag{4}$$

The physical boundary conditions are given by:

$$\begin{aligned} &u \to U_w, \quad v = v_w, \quad T = T_w, \quad C = C_w, && \text{at } y = 0, \\ &u \to U_e, \quad T \to T_\infty, \quad C \to C_\infty, && \text{at } y \to \infty, \end{aligned} \tag{5}$$

where $U_w(x)$ is the stretching sheet velocity, $U_e(x)$ is the free stream velocity, $v_w$ is the suction/ injection, and $q'''$ is the rate of non-uniform heat source/sink, as defined below:

$$U_w(x) = U_0 \exp\left(\frac{x}{L}\right),\ U_e(x) = U_\infty \exp\left(\frac{x}{L}\right),\ v_w = v_o \exp\left(\frac{x}{2L}\right),\ \text{and}\ q''' = \frac{kU_w}{x\upsilon}\left[A^*(T_w - T_\infty)F + B^*(T - T_\infty)\right], \tag{6a}$$

where $U_0$ is the reference velocity, $U_\infty$ is the free stream velocity, $L$ is the characteristic length, $v_o$ is constant, $A^*$ is the space-dependent heat source/sink, and $B^*$ is the temperature-dependent heat source/ sink. We introduce the non-similar transformations,

$$\begin{aligned} &\xi = \frac{x}{L},\ \eta = \left(\frac{U_0}{\nu x}\right)^{1/2} \exp\left(\frac{x}{2L}\right) y,\ \psi(x,y) = (\nu U_o x)^{1/2} \exp\left(\frac{x}{2L}\right) f(\xi,\eta), \\ &T - T_\infty = (T_w - T_\infty) G(\xi,\eta),\ (T_w - T_\infty) = (T_{w0} - T_\infty) \exp\left(\frac{2x}{L}\right), \end{aligned} \tag{6b}$$

$$C-C_\infty=(C_w-C_\infty)H(\xi,\eta),\ (C_w-C_\infty)=(C_{w0}-C_\infty)\exp\left(\frac{2x}{L}\right),$$

$$u=\frac{\partial\psi}{\partial y},\ v=-\frac{\partial\psi}{\partial x},\ u=U_0\exp\left(\frac{x}{L}\right)F, \tag{6c}$$

$$v=-\left(\frac{\nu U_0}{x}\right)^{1/2}\exp\left(\frac{x}{2L}\right)\left\{(1+\xi)\frac{f}{2}+\xi f_\xi+\frac{\eta}{2}(\xi-1)\frac{\partial f}{\partial\eta}\right\}.$$

By substituting Eq. (6) into Eqs. (1) - (4), we find that Eq. (1) is satisfied identically, and Eqs. (2) and (3) are reduced to the following Eqs.:

$$F_{\eta\eta}+(1+\xi)\frac{f}{2}F_\eta+\xi Ri(G+NH)-\xi F^2+\xi M^2e^{-\xi}\,\mathrm{Re}(\varepsilon-F)=\xi(FF_\xi-f_\xi F_\eta) \tag{7}$$

$$G_{\eta\eta}+(1+\xi)\frac{\mathrm{Pr}\,f}{2}G_\eta-2\xi\,\mathrm{Pr}\,FG+(A^*F+B^*G)+\xi\,\mathrm{Pr}\,M^2e^{-\xi}\,\mathrm{Re}\,Ec(\varepsilon-F)^2=\xi\,\mathrm{Pr}(FG_\xi-f_\xi G_\eta) \tag{8}$$

$$H_{\eta\eta}+(1+\xi)\frac{Scf}{2}H_\eta-2\xi ScFH=\xi Sc(FH_\xi-f_\xi H_\eta) \tag{9}$$

The transformed boundary conditions are given by:

$$\begin{aligned}&F(\xi,0)=1,\quad G(\xi,0)=1,\quad H(\xi,0)=1,\quad \text{at}\ \ \eta=0,\\&F(\xi,\eta)=\varepsilon,\quad G(\xi,\eta)=0,\quad H(\xi,\eta)=0,\quad \text{at}\ \ \eta\to\infty.\end{aligned} \tag{10}$$

Here $f(\xi,\eta)=\int_0^\eta F.d\eta+f_w$ and $f_w$ can be obtained from the following equation: $(1+\xi)f_w/2+\xi f_\xi=A\xi^{1/2}$, where $A=-v_0(L/\nu U_0)^{1/2}$ = constant, is the surface mass transfer parameter with $A$> 0 for suction, $A$< 0 for injection and $A$ = 0 for an impermeable surface. The Richardson number ($Ri$) or mixed convection parameter which gives the strength of the comparative natural and forced convections, where $Ri=0$ corresponds to the purely forced convection case and $Ri\to\infty$ corresponds to the free convection case. The relative measure of buoyancy forces of temperature and concentration gradients is denoted by the dimensionless parameter ($N$), $\varepsilon$ is the ratio of velocity parameter. Further, $Re$ denotes the Reynolds number, $M$ denotes the magnetic field parameter, and $Ec$ denotes the Eckert number.

$$Ri=\frac{Gr}{\mathrm{Re}^2},\ N=\frac{Gr^*}{Gr},\ \varepsilon=\frac{U_\infty}{U_0},\ \mathrm{Re}=\frac{LU_0}{\nu},\ M=\frac{B_0^2\sigma\nu}{U_0^2\rho}\ \text{and}\ Ec=\frac{U_0^2}{C_p(T_{w_o}-T_\infty)}. \tag{11}$$

The skin friction coefficient $C_f$, the Nusselt number $Nu$ and the Sherwood number $Sh$ are the most interesting physical quantities, which are defined below:

$$C_f=\mu\frac{2(\partial u/\partial y)_{y=0}}{\rho U_w^{\,2}}=2\left(\mathrm{Re}\,\xi\exp(\xi)\right)^{-1/2}F_\eta(\xi,0),\ \ \text{i.e.,}\ \left(\mathrm{Re}\,\xi\exp(\xi)\right)^{1/2}C_f=2F_\eta(\xi,0). \tag{12}$$

$$Nu=-x\frac{(\partial T/\partial y)_{y=0}}{(T_w-T_\infty)}=-\left(\mathrm{Re}\,\xi\exp(\xi)\right)^{1/2}G_\eta(\xi,0),\ \ \text{i.e.,}\ \left(\mathrm{Re}\,\xi\exp(\xi)\right)^{-1/2}Nu=-G_\eta(\xi,0). \tag{13}$$

$$Sh=-x\frac{(\partial C/\partial y)_{y=0}}{(C_w-C_\infty)}=-\left(\mathrm{Re}\,\xi\exp(\xi)\right)^{1/2}H_\eta(\xi,0),\ \ \text{i.e.,}\ \left(\mathrm{Re}\,\xi\exp(\xi)\right)^{-1/2}Sh=-H_\eta(\xi,0). \tag{14}$$

## 3. Method of Solution

Using an implicit finite difference scheme combined with the quasilinearization technique, the set of dimensionless partial differential equations (7)-(9) associated with the boundary conditions (10) has been solved. Hence, we apply the quasilinearization technique [39-40] to the nonlinear coupled system of partial differential equations, then they are replaced by the following sequence of linear partial differential equations:

$$F_{\eta\eta}^{i+1} + A_1^i F_\eta^{i+1} + A_2^i F^{i+1} + A_3^i F_\xi^{i+1} + A_4^i G^{i+1} + A_5^i H^{i+1} = A_6^i, \tag{15}$$

$$G_{\eta\eta}^{i+1} + B_1^i G_\eta^{i+1} + B_2^i G^{i+1} + B_3^i G_\xi^{i+1} + B_4^i F^{i+1} = B_5^i, \tag{16}$$

$$H_{\eta\eta}^{i+1} + C_1^i H_\eta^{i+1} + C_2^i H^{i+1} + C_3^i H_\xi^{i+1} + C_4^i F^{i+1} = C_5^i. \tag{17}$$

The functions of (i+1)$^{th}$ iterations are unknown, and need to be determined while the coefficient function of the i$^{th}$ iteration are known. The boundary conditions (10) are as follows:

$$\begin{aligned} &F^{i+1}(\xi,0)=1, \quad G^{i+1}(\xi,0)=1, \quad H^{i+1}(\xi,0)=1, \quad \text{at} \quad \eta=0, \\ &F^{i+1}(\xi,\eta)=\varepsilon, \quad G^{i+1}(\xi,\eta)=0, \quad H^{i+1}(\xi,\eta)=0, \quad \text{at} \quad \eta=\eta_\infty. \end{aligned} \tag{18}$$

The coefficients in equations (15-17) are given by:

$$\begin{aligned} A_1^i &= (1+\xi)\frac{f}{2} + \xi f_\xi, \\ A_2^i &= -\xi(2F + ReM^2 e^{-\xi} + F_\xi), \\ A_3^i &= -\xi F,\ A_4^i = \xi Ri,\ A_5^i = \xi RiN, \\ A_6^i &= -\xi\left(\left(F + F_\xi\right)F + M^2 Re\varepsilon e^{-\xi}\right). \\ B_1^i &= (1+\xi)\frac{\Pr f}{2} + \xi \Pr f_\xi, \\ B_2^i &= -(2\xi \Pr F - B^*),\ B_3^i = -\xi \Pr F, \\ B_4^i &= -\Pr\xi(2G + G_\xi + 2e^{-\xi} M^2 \operatorname{Re} Ec(\varepsilon - F)) + A^*, \\ B_5^i &= -\xi \Pr F(2G + G_\xi) - \xi \Pr M^2 \operatorname{Re} e^{-\xi} Ec(\varepsilon^2 - F^2). \\ C_1^i &= (1+\xi)\frac{Scf}{2} + \xi Scf_\xi, \\ C_2^i &= -2\xi ScF,\ C_3^i = -\xi ScF, \\ C_4^i &= -Sc\xi(2H + H_\xi), C_5^i = C_4^i F. \end{aligned} \tag{19}$$

The resulting sequence of linear partial differential equations (15)-(17) was discretized using a second-order central difference formula in the $\eta$-direction (boundary layer) and a backward difference formula in the $\xi$-direction (streamwise). At each iteration step, the equations were then reduced to a system of linear algebraic equations, with block tridiagonal structure, which was then solved by using Varga's algorithm [44]. To assure convergence, the absolute value between two successive iterations is taken to be $10^{-5}$:

$$\text{i.e.,}\ Max\left\{\left|\left(f_{\eta\eta}\right)_w^{i+1} - \left(f_{\eta\eta}\right)_w^i\right|, \left|\left(G_\eta\right)_w^{i+1} - \left(G_\eta\right)_w^i\right|, \left|\left(H_\eta\right)_w^{i+1} - \left(H_\eta\right)_w^i\right|\right\} \le 10^{-5} \tag{20}$$

The results in the current study are compared with the results obtained by Magyari and Keller [22], Bidin and Nazar [23] and Mukhopadhyay [24] in the Table 1 for different values of *Pr*, and are found to be in good agreement. In support of nonsimilar solutions, the numerical results for the skin friction coefficient, heat and mass transfer rates are displayed in the Table 2.

**Table 1.** Comparison of the steady state results $[-G_\eta(0)]$ for $Ri=0,\ N=0,\ \varepsilon=0,\ A^*=0,\ B^*=0,\ A=0,\ Ec=0$, $M=0$ and for selected values of $Pr$ to previously published work.

| *Pr* | Magyari and Keller [22] | Bidin and Nazar [23] | Mukhopadhyay [24] | Current results |
|---|---|---|---|---|
| 1 | 0.9548 | 0.9547 | 0.9547 | 0.9541 |
| 3 | 1.8691 | 1.8691 | 1.8691 | 1.8691 |
| 5 | 2.5001 | - | 2.5001 | 2.5014 |
| 6 | 3.6604 | - | 3.6603 | 3.6698 |

## 4. Results and Discussion

The non-dimensional equations (7) – (9) with the boundary conditions (10) have been solved numerically by using the implicit finite difference method in conjunction with the quasilinearization technique. The results are obtained to show the influence of the non-dimensional governing parameters, namely, the streamwise co-ordinate $\xi$, magnetic field parameter $M$, mixed convection parameter (Richardson number) $Ri$, ratio of buoyancy forces parameter $N$, velocity ratio parameter $\varepsilon$, space-dependent heat source/ sink parameter $A^*$, temperature-dependent heat source/ sink $B^*$, Eckert number $Ec$, suction/ injection parameter $A$, and Schmidt number $Sc$ on the velocity, temperature and species concentration fields. The range of non-dimensional parameters utilized in the research paper may differ in accordance to the physical situation that arises during mathematical modelling of the considered problem. The values of the non-dimensional parameters are taken in concern with the physical properties of water. For instance, at 20 $^0$C, for water, $Pr$ = 7.0 and $\nu$ = 1.004 * $10^{-2}$ cm$^2$/s etc.

**Table 2.** Steady state results of skin friction coefficient $\mathrm{Re}^{1/2} C_f$, heat transfer rate $\mathrm{Re}^{-1/2} Nu$ and mass transfer rate $\mathrm{Re}^{-1/2} Sh$ for $Pr$ = 7.0, $N$ = 1.0, $Sc$ = 2.57, $Ri$ =10.0, $\xi = 1$ and $Re$ =10.0.

| $M$ | $\varepsilon$ | $A$ | $A^*$ | $B^*$ | $Ec$ | $\mathrm{Re}^{1/2} C_f$ | $\mathrm{Re}^{-1/2} Nu$ | $\mathrm{Re}^{-1/2} Sh$ |
|---|---|---|---|---|---|---|---|---|
| 0.0 | 0.5 | 0.5 | 0.5 | 0.5 | 0.5 | 4.233836 | 6.07180 | 1.5101 |
| 1.0 | 0.5 | 0.5 | 0.1 | 0.5 | 0.5 | 3.13048 | 4.61590 | 1.4656 |
| 1.0 | 0.5 | 0.5 | 0.1 | 0.5 | 0.5 | 3.13048 | 4.61590 | 1.4656 |
| 1.0 | 1.0 | 0.5 | 1.0 | 0.5 | 0.5 | 4.24540 | 5.92125 | 1.5300 |
| 1.0 | 1.5 | 0.5 | 1.0 | 0.5 | 0.5 | 5.93578 | 5.89412 | 1.6049 |
| 1.0 | 0.5 | 1.0 | 1.0 | 0.5 | 0.5 | 5.34596 | 1.00216 | 1.1256 |
| 1.0 | 0.5 | 0.0 | 0.1 | 0.5 | 0.5 | 4.10534 | 2.6755 | 1.3374 |
| 1.0 | 0.5 | 1.0 | 0.1 | 0.5 | 0.5 | 2.14652 | 7.29975 | 1.6224 |
| 1.0 | 0.5 | 0.5 | 0.5 | 0.5 | 0.5 | 2.56134 | 5.30424 | 1.4359 |
| 1.0 | 0.5 | 0.5 | 0.0 | 0.5 | 0.5 | 2.84274 | 4.96478 | 1.4508 |
| 1.0 | 0.5 | 0.5 | 0.5 | 0.5 | 0.5 | 3.13048 | 4.61590 | 1.4656 |
| 1.0 | 0.5 | 0.5 | 0.5 | 0.5 | 0.5 | 3.03893 | 4.81471 | 1.4622 |
| 1.0 | 0.5 | 0.5 | 0.5 | 0.0 | 0.5 | 3.08324 | 4.71742 | 1.4639 |
| 1.0 | 0.5 | 0.5 | 0.5 | 0.5 | 0.5 | 3.13048 | 4.61590 | 1.4656 |
| 1.0 | 0.5 | 0.5 | 0.5 | 0.5 | 1.0 | 1.48849 | 7.85298 | 1.3954 |
| 1.0 | 0.5 | 0.5 | 0.5 | 0.5 | 0.0 | 2.41405 | 2.80220 | 1.5023 |
| 1.0 | 0.5 | 0.5 | 0.5 | 0.5 | 1.0 | 4.13335 | 5.95562 | 1.4346 |

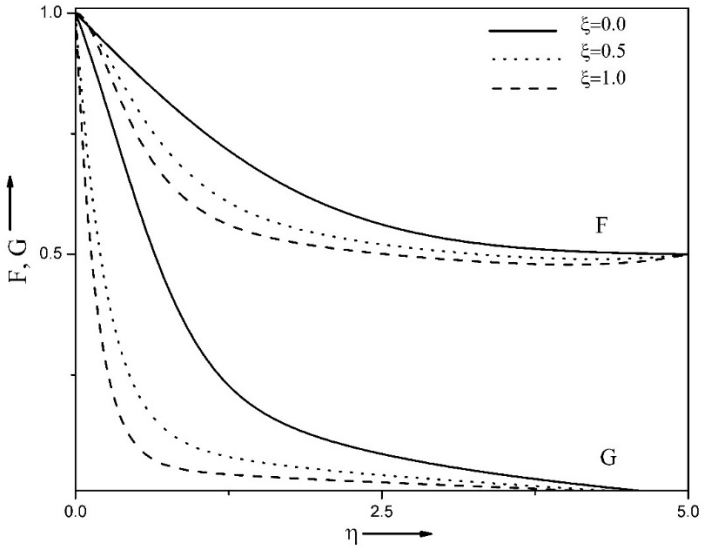


**Fig. 2.** Effect of non-similar variable $\xi$ on F ($\xi$ , $\eta$) and G($\xi$ , $\eta$) for Pr = 7.0, Re=10.0, N=1.5, Sc=2.57, $\varepsilon$ = 0.5, A = 0.5, Ec = 0.1, Ri =10.0, A*= 0.5, B*= 0.5 and M=1.0.

Figure 2 demonstrates the role of the streamwise co-ordinate $\xi$ on the velocity $F(\xi,\eta)$ and temperature $G(\xi,\eta)$ profiles at $A = 0.5$, $Ec = 0.1$, $Pr = 7.0$, $\mathrm{Re} = 10.0$, $N = 1.5$, $Sc = 2.57$, $Ri = 10.0$, $\varepsilon = 0.5$, $A^* = 0.5$, $B^* = 0.5$ and $M = 1.0$. It is observed that the velocity and temperature profiles decrease with the increase of the streamwise co-ordinate $\xi$ from 0 to 1. The velocity and temperature profiles decrease approximately 8% and 51% as the streamwise co-

ordinate $\xi$ increases from 0 to 1, respectively. This clearly indicates that the streamwise co-ordinate $\xi$ significantly influences the flow, thermal, and in turn the species concentration fields, and also shows the existence of non-similarity solutions.

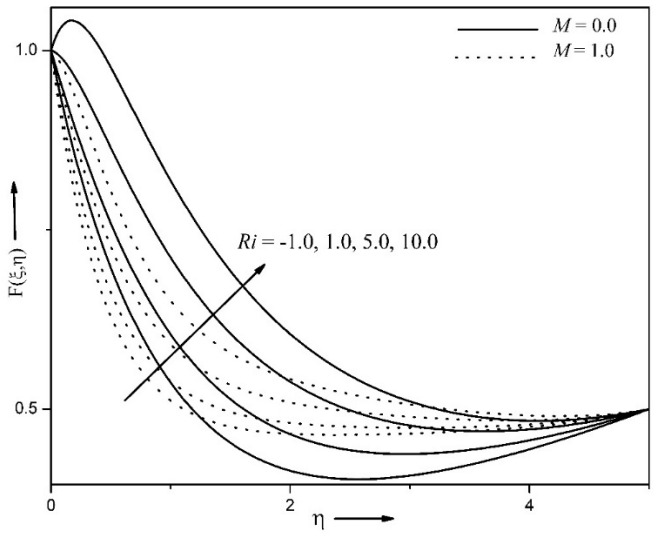


**Fig. 3.** Effect of Ri and M on F ( $\xi$ , $\eta$ ) for Pr= 7.0, Re=10.0, A= 0.5, N=0.5, Sc=0.66, Ec=0.1, $\varepsilon$ = 0.5, A*=0.5, B*= 0.5 and $\xi$ =0.5.

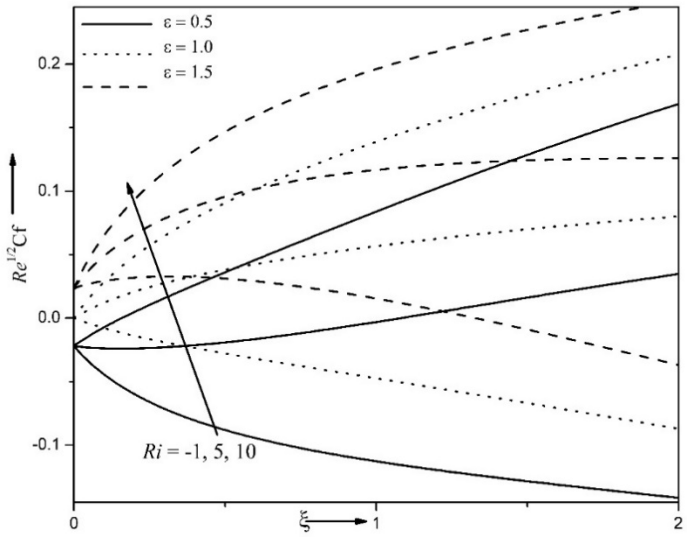


**Fig. 4.** Effect of $\varepsilon$ and Ri on $\mathrm{Re}^{1/2}\,Cf$ for Pr= 7.0, Re=10.0, N=0.5, Sc=0.66, A* = 0.5, Ec=0.1, A = 0.5, M = 0.5 and B*= 0.1.

The effects of the mixed-convection parameter $(Ri)$ and the magnetic field parameter $M$ on the velocity profile $F(\xi,\eta)$ are shown in Fig. 3 for $Pr = 7.0$, $\varepsilon = 0.5$, $A^* = 0.5$, $\mathrm{Re} = 10.0$, $A = 0.5$, $N = 0.5$, $Sc = 0.66$, $Ec = 0.1$, $B^* = 0.5$ and $\xi = 0.5$. It is observed that an increase in the value of $Ri$ has the tendency to increase the buoyancy effect, and hence the velocity profile increases. For buoyancy-opposing force $(Ri < 0)$, the velocity profile decreases, whereas for buoyancy-aiding force $(Ri > 0)$, the magnitude of the velocity profile increases. The physical reason is that the assisting buoyancy force due to the thermal gradients acts like sufficient pressure gradient and that enhances the fluid acceleration and increases the magnitude of the velocity profile within the momentum boundary layer. It is clearly observed from Fig. 3 that, in the presence of the magnetic field parameter, the velocity profile decreases as compared to the velocity profile in its absence. This is due to the fact that application of the magnetic field parameter normal to the flow of an electrically conducting fluid gives rise to a resistive force, called the Lorentz force that acts in the opposite direction to the flow one. Thus, the momentum boundary layer thickness decreases significantly when the magnetic field is considered.

Figure 4 depicts the effects of the velocity ratio parameter $(\varepsilon)$ and buoyancy parameter $(Ri)$ on the skin friction

coefficient $(\mathrm{Re}^{1/2}Cf)$ for $Pr=7.0$, $A^*=0.5$, $\mathrm{Re}=10.0$, $A=0.5$, $N=0.5$, $Sc=0.66$, $Ec=0.1$, $B^*=0.1$, and $M=0.5$. It reveals that $\mathrm{Re}^{1/2}Cf$ increases near the wall for both values of $\varepsilon$ i.e., $\varepsilon=1.0$ and $\varepsilon=1.5$. Note that $\mathrm{Re}^{1/2}Cf$ decreases for $\varepsilon=0.5$, due to the fact that the stretching velocity $U_w$ is dominating over the free stream velocity $U_e$.

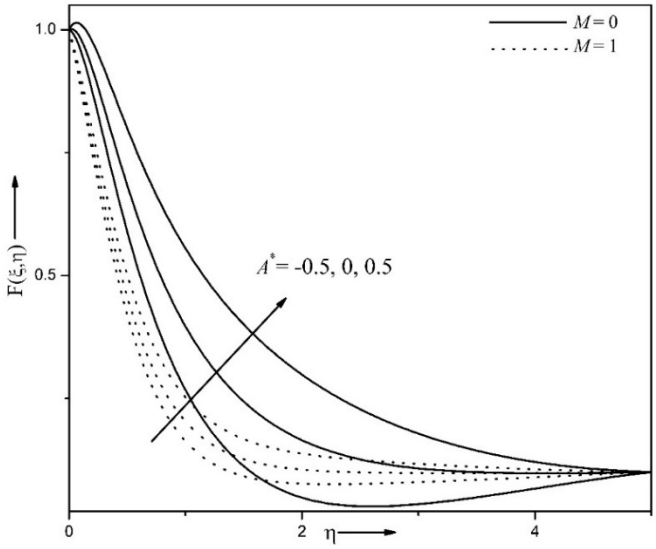


**Fig. 5.** Effect of M and A* on F ( $\xi$ , $\eta$ ) for Pr= 7.0, Re=10.0, Ri = 10.0, N=0.5, Sc=0.94, A =0.5, Ec = 0.5, $\varepsilon$ = 0.1, B* = 0.1 and $\xi$ = 0.5.

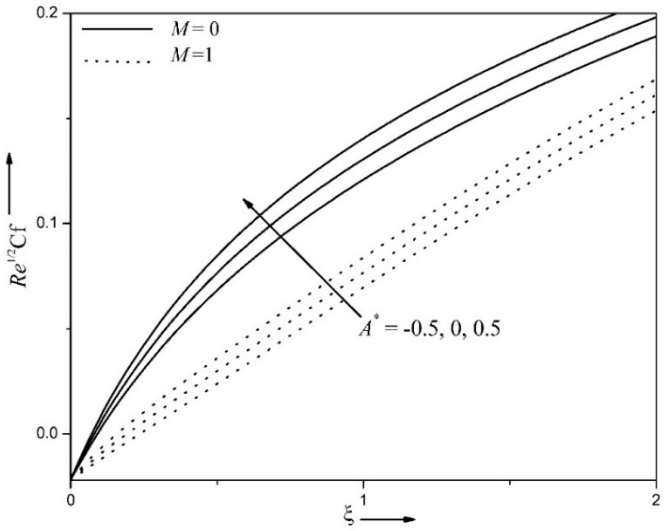


**Fig. 6.** Effect of M and A* on $\mathrm{Re}^{1/2}Cf$ for Pr =7.0, Re =10.0, Ri = 10.0, N = 0.5, Sc = 0.94, A = 0.5, Ec = 0.5, $\varepsilon$ = 0.1 and B*= 0.1.

The influence of the buoyancy-assisting force $(Ri>0)$ increases the skin friction coefficient monotonously, for all the values of $\varepsilon$ , i.e., $\varepsilon=0.5$, $\varepsilon=1.0$ and $\varepsilon$=1.5. It is observed that the skinfriction coefficient $(\mathrm{Re}^{1/2}C_f)$ increases with increase of mixed convection parameter $Ri$ accountably. This is due to the increase of $(Ri)$ that enhances the fluid acceleration and results in thinner momentum boundary layer. Thus, the skinfriction coefficient $(\mathrm{Re}^{1/2}C_f)$ increases. In particular, $|(\mathrm{Re}^{1/2}Cf)|$ increases approximately 97% and 68% as $Ri$ increases from $Ri=-1$ to $Ri=5$, at $\varepsilon=0.5$ and $\varepsilon$=1.0, respectively.

The effects of the space-dependent heat source/ sink parameter $A^*$ and magnetic field parameter $M$ on the velocity profile $F(\xi,\eta)$ and skin friction coefficient $(\mathrm{Re}^{1/2}Cf)$ are displayed in Figs. 5 and 6, for $A=0.5$, $\mathrm{Pr}=7.0$, $\mathrm{Re}=10.0$, $Sc=0.94$, $\varepsilon=0.1, B^*=0.1$ $Ri=10.0$, $N=0.5$ and $Ec=0.5$. It is inferred from Fig. 5 that, in the presence of the magnetic field parameter $M$, for $A^*>0$ (in the presence of a space-dependent heat source effect), the momentum boundary layer increases near the wall and decreases gradually away from the wall. On other hand, for $A^*<0$ (in the presence of a space-dependent heat sink effect), the velocity profile decreases at the wall. In the presence of the magnetic

field parameter, the velocity profile decreases because of the resistive force, *i.e.* the Lorentz force, which has a tendency to slow down the motion of the fluid in the boundary layer. However, in the absence of the magnetic field parameter $M$, the velocity profile increases with $A^*$, in contrast to the case where the magnetic field parameter $M$ is present. From the Fig. 6, it is obvious that the skin friction coefficient increases monotonously for $A^* > 0$ (in the presence of a space-dependent heat source effect), where it decreases for $A^* < 0$ (in the absence of a space-dependent heat sink effect). It is worthy of note that the skin friction coefficient increases in the absence of a magnetic field as compared to the case of without magnetic field. In particular, $\mathrm{Re}^{1/2} Cf$ increases about 16% and 20% as $A^*$ increases from $A^* = -0.5$, to $A^* = 0.5$ at $M = 0$ and $M = 1$, respectively.

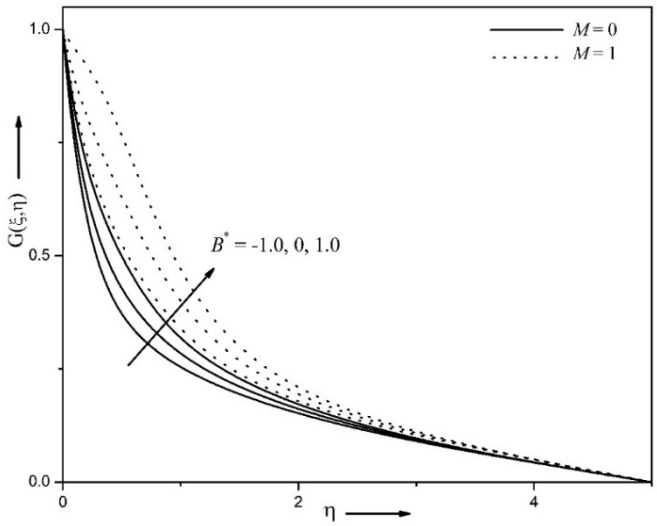


**Fig. 7.** Effect of M and B* on $G(\xi, \eta)$ for Pr = 7.0, Re = 10.0, Ri = 10.0, N=1.0, Sc = 0.66, A =0.5, $\varepsilon$ = 0.5, A*= 0.5, Ec = 0.1 and $\xi$ = 0.5.

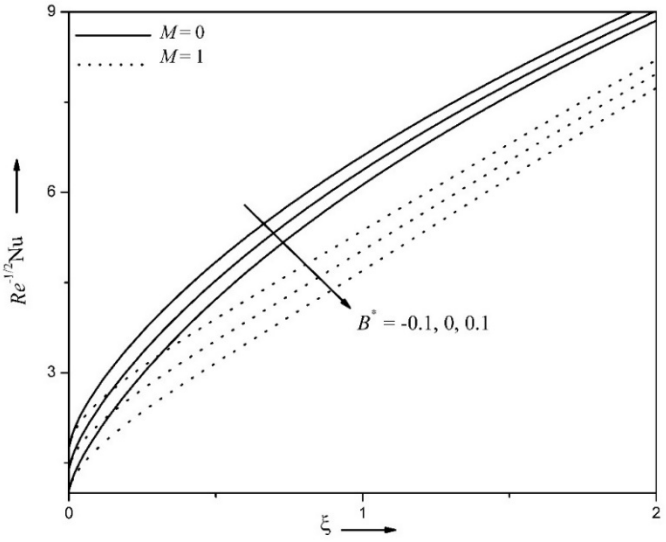


**Fig. 8.** Effect of M and B*on Heat transfer rate for Pr =7.0, Re =10.0, Ri = 10.0, N = 0.5, Sc = 0.66, A = 0.5, Ec = 0.1, $\varepsilon$ = 0.5 and A*= 0.5.

Figures 7 and 8 show the effect of temperature-dependent heat source/ sink $B^*$ and magnetic field parameter $M$ on the temperature profile $G(\xi, \eta)$ and heat transfer rate $(\mathrm{Re}^{-1/2} Nu)$, for a constant value of $\mathrm{Pr} = 7.0$, $\mathrm{Re} = 10.0$, $Ri = 10.0$, $N = 1.0$, $Sc = 0.66$, $A^* = 0.5$, $A = 0.5$, $Ec = 0.1$ and $\varepsilon = 0.5$. The heat generation/ absorption clearly affects the fluid temperature. It is the cumulative influence of the temperature-dependent heat source/ sink parameter that determines the extent to which temperature falls/ rises within the thermal boundary layer. From the Figs it is clear that, for the temperature dependent heat source effect $(B^* > 0)$, energy is released and hence the magnitude of the temperature increases, whereas for the temperature-dependent heat sink effect $(B^* < 0)$, energy is absorbed and hence the magnitude of the temperature decreases. Non-uniform heat sink contributes to quenching the heat from the stretching sheet

significantly. From Fig. 7, it can be seen that the temperature of the fluid adjacent to the surface increases as the magnetic field parameter increases, while the effect is not much significant far away from the plate. Also from Fig. 8, it is obvious that the heat transfer rate $(\mathrm{Re}^{-1/2} Nu)$ decreases for $B^* > 0$ (heat source effect) and increases for $B^* < 0$ (heat sink effect). It is worthy of mention that the heat transfer rate decreases in the presence of the magnetic field parameter, as compared to in its absence. In particular, the heat transfer rate decreases around 48% and 12% as $B^*$ increases from $B^* = -0.1$ to $B^* = 0.1$, at $M = 0$ and $M = 1$, respectively.

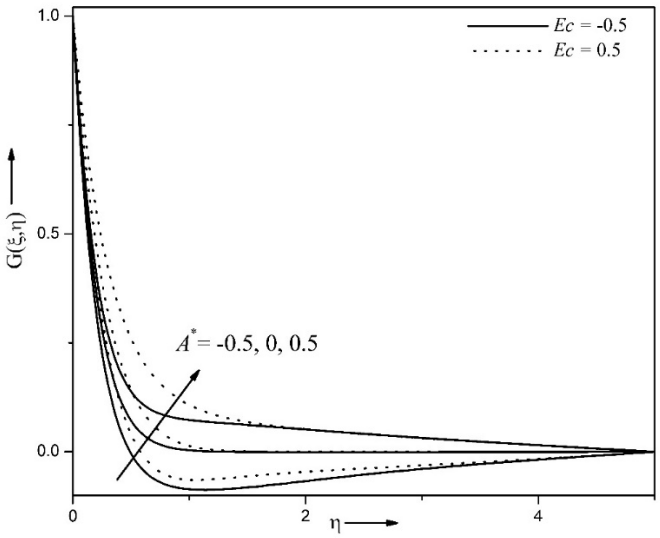


**Fig. 9.** Effect of Ec and A* on $G(\xi, \eta)$ for Pr = 7.0, Re = 10.0, Ri = 10.0, N = 0.5, Sc = 0.66, A = 0.5, M =1.0, $\varepsilon$ = 0.5, B*= 0.2 and $\xi$ = 0.5.

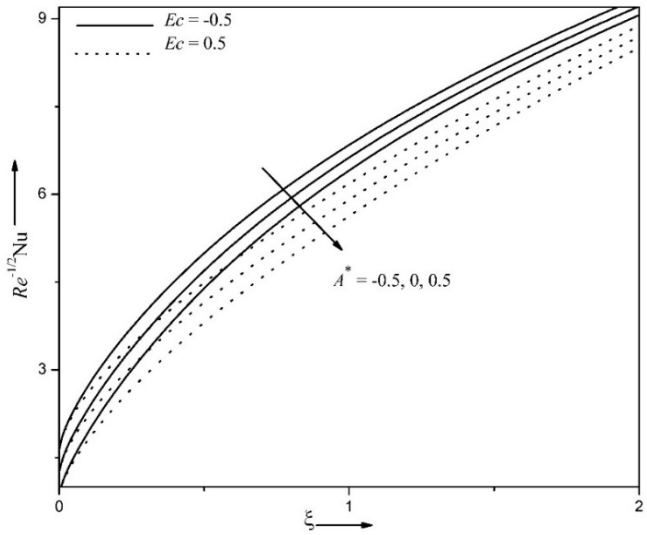


**Fig. 10.** Effect of Ec and A* on Heat transfer rate for Pr =7.0, Re =10.0, Ri = 10.0, N = 0.5, Sc = 0.66, A = 0.5, M = 1.0, $\varepsilon$ = 0.5 and B* = 0.2.

Figures 9 and 10 present the effects of different values of the Eckert number $Ec$ and space-dependent heat source/sink parameter $A^*$ on the temperature profile and rate of heat transfer $(\mathrm{Re}^{-1/2} Nu)$, respectively, for $\mathrm{Pr} = 7.0$, $\mathrm{Re} = 10.0$, $Ri = 10.0, N = 0.5$, $Sc = 0.66, B^* = 0.2, A = 0.5, M = 1.0$ and $\varepsilon = 0.5$. It is clear from Fig. 9 that the temperature profile increases for a space-dependent heat source effect ( $A^* > 0$ ). Due to the increase of the value of $A^*$, the energy is released, leading to an increase in the fluid temperature within the thermal boundary layer. On the contrary, for a space-dependent heat sink effect ($A^* < 0$), energy is absorbed, and as a result, the temperature drops significantly within the thermal boundary layer. It is important to note that, with an increase in the value of $Ec$, the dimensionless temperature as well as the thickness of the boundary layer increases, due to heat addition by means of frictional heating. From Fig. 10, it is clear that the heat transfer rate $(\mathrm{Re}^{-1/2} Nu)$, decreases with an increasing value of the heat source effect ( $A^* > 0$ ), while it increases with an increasing value of the heat sink effect $(A^* < 0)$. The effect of increasing $Ec$ is to decrease the rate of

heat transfer. Thus, by varying the Eckert number, the temperature distribution as well as the heat transfer rate can be manipulated. In particular, $\mathrm{Re}^{-1/2} Nu$, decreases by 6% and 9%, as $A^*$ increases from $A^* = -0.5$, to $A^* = 0.5$ at $Ec = -0.5$ and $Ec = 0.5$, respectively.

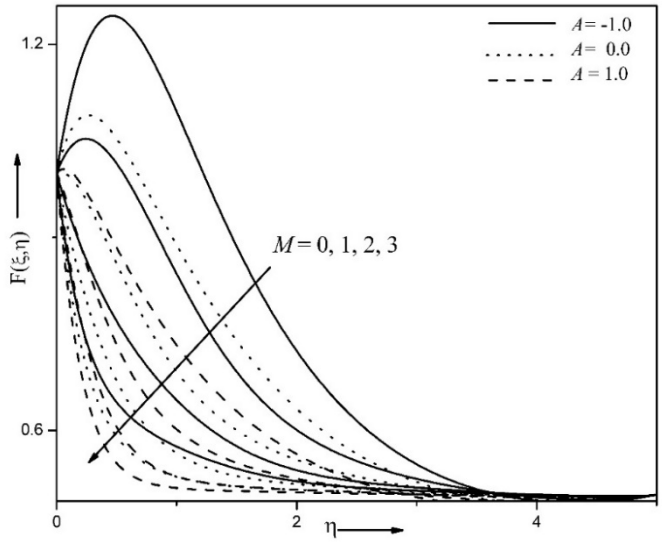


**Fig. 11.** Effect of M and A on $F(\xi,\eta)$ for Pr = 7.0, Re = 10.0, Ri = 10.0, N = 1.0, Sc = 0.94, A* =0.5, Ec=0.1, $\varepsilon$ = 0.5, B*= 0.1 and $\xi$ = 0.5.

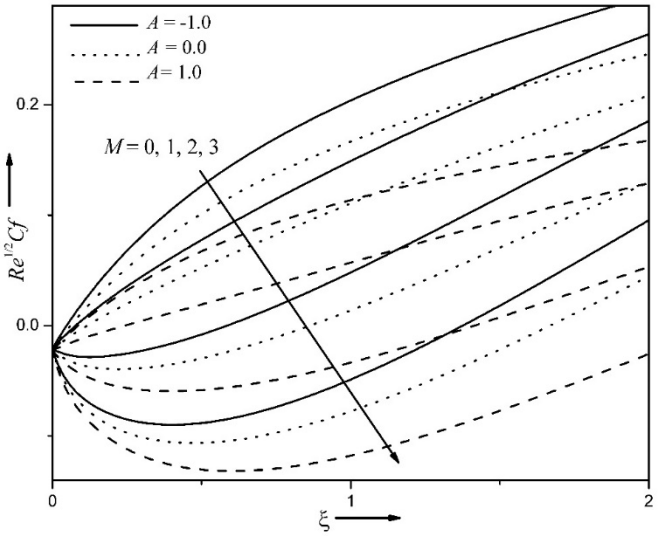


**Fig. 12.** Effect of M and A on $\mathrm{Re}^{1/2} Cf$ for Pr = 7.0, Re = 10.0, Ri = 10.0, N=1.0, Sc=0.94, A* = 0.5, Ec=0.1, $\varepsilon$ = 0.5 and B*= 0.1.

Figures 11 and 12 present the effect of the magnetic field parameter $M$ with the suction/ injection parameter $A$ on the velocity profile $F(\xi,\eta)$, and skin friction coefficient parameter $(\mathrm{Re}^{1/2} Cf)$, respectively, for a fixed values of $\mathrm{Pr} = 7.0$, $\mathrm{Re} = 10.0$, $Ri = 10.0$, $N = 1.0$, $Sc = 0.94$, $B^* = 0.1$, $A^* = 0.5$, $Ec = 0.1$, $\varepsilon = 0.5$. The results indicate that a high-velocity overshoot is observed near the wall of the exponentially stretching sheet for injection ( $A < 0$ ), and increased injection tends to enhance the boundary layer thickness. The case $A = 0$ represents the impermeable stretching sheet. On the other hand, the overshoot is reduced for suction ( $A > 0$ ) and the boundary layer becomes thinner, and the velocity profile is reduced. Thus it is evident that velocity adjacent to the wall can be manipulated through the suction/ injection parameter. From Fig. 11, it is obvious that the overshoot occurs in the absence of a magnetic field, and the overshoot gradually decreases as the magnetic field increases. It is evident that an increase in the magnetic field parameter decreases the fluid velocity adjacent to the wall. Moreover, the absence of the magnetic parameter can increase fluid velocity both inside and adjacent to the wall effectively. We observe from Fig. 12 that the skin friction coefficient increases monotonously as the injection $(A < 0)$ effect is induced, while the reverse trend is noticed when the suction $(A > 0)$ is induced. The skin

friction coefficient increases in the absence of magnetic field parameter as compared in absence of magnetic field parameter. In particular, $(Re^{1/2}Cf)$ decreases around 26% and 50%, as $M$ increases from $M=0$ to $M=1$, at $A=-1.0$ and $A=1.0$, respectively.

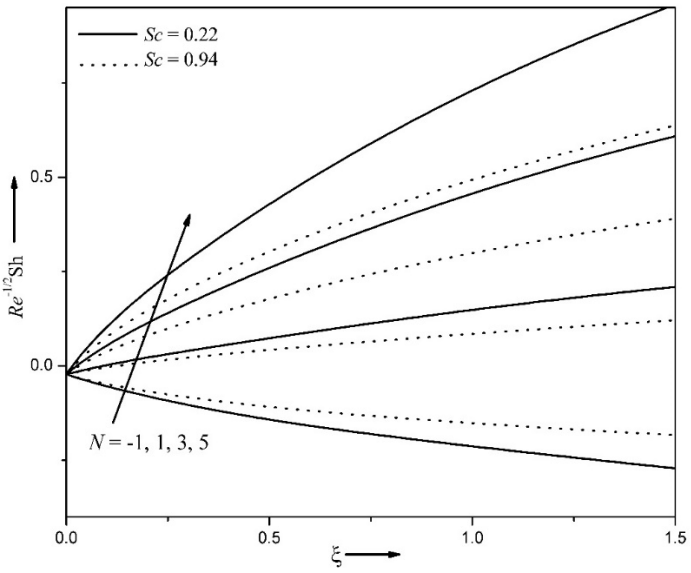


**Fig. 13.** Effect of N and Sc on mass transfer rate for Pr= 7.0, Re=10.0, Ri = 10.0, M = 1.0, A = 1.0, Ec=0.5, $\varepsilon$ = 0.5, A*= 0.5 and B*= 0.5.

Figure 13 represents the behavior of the Schmidt number $(Sc)$ and the ratio of buoyancy forces parameter $(N)$ on the mass transfer rate $(Re^{-1/2}Sh)$ for $\mathrm{Re}=10.0$, $\mathrm{Pr}=7.0$, $Ri=10.0$, $A=1.0$, $M=1.0$, $B^*=0.5$, $A^*=0.5$, $Ec=0.5$ and $\varepsilon=0.5$. It is observed from Fig. 13 that the mass transfer rate increases as the ratio of buoyancy forces parameter $(N)$ increases. The physical reason is that the assisting ratio of buoyancy forces $(N>0)$ implies a favorable pressure gradient, and thus fluid gets accelerated. Consequently, the mass transfer rate increases. On the contrary, the mass transfer rate $(\mathrm{Re}^{-1/2}\,Sh)$ decreases for the opposite ratio of buoyancy forces $(N<0)$. Moreover, it is important to note that, as the Schmidt number increases, the mass transfer rate $(\mathrm{Re}^{-1/2}\,Sh)$ decreases. To be more specific, $(\mathrm{Re}^{-1/2}\,Sh)$ increases about 207% and 251% as $N$ increases from $N=1$ to $N=3$, at $Sc=0.22$ and $Sc=0.94$, respectively.

## 5. Conclusions

The present study explores the comprehensive numerical investigation for non-similar solutions of steady MHD mixed convection over an exponentially stretching surface in the presence of a non-uniform heat source or sink and suction/ injection effects. The following conclusions are drawn from the present numerical investigation:

1. The streamwise co-ordinate $\xi$ significantly influences flow, thermal and species concentration fields, and displays the existence of non-similarity solutions.
2. The effect of the magnetic field parameter and the suction parameter is to reduce the velocity profile, while increasing the temperature profile.
3. The magnitude of the skin friction coefficient increases approximately 97% and 68% as the velocity ratio parameter $\varepsilon$ increases from 0.5 to 1.5 at $Ri=-1$ and $Ri=5$, respectively.
4. The space- and temperature-dependent heat source/sink parameters tend to increase the temperature profile for heat generation conditions while they decrease the temperature profile for absorption conditions. Also, due to the increase in the value of $Ec$ , the dimensionless temperature as well as the thickness of the boundary layer increase.
5. As the Schmidt number increases, the mass transfer rate $(\mathrm{Re}^{-1/2}\,Sh)$ decreases. Particularly, $(\mathrm{Re}^{-1/2}\,Sh)$ increases about 207% and 251% as $N$ increases from $N=1$ to $N=3$, at $Sc=0.22$ and $Sc=0.94$, respectively.

## Conflict of Interest

The authors declared no potential conflicts of interest with respect to the research, authorship and publication of this article.

## Funding

Prof. P.M. Patil thanks the University Grants Commission, New Delhi, India for its financial assistance under the MRP grant: F. No. 43-413/2014 (SR), dated 30-10-2015.

## References

[1] Alfven, H., Existence of electromagnetic-hydrodynamic waves, *Nature*, 150 (1942) 405.
[2] Ahmed, S., Zueco, J., Luis, M., Gonzalez, L., Effects of chemical reaction, heat and mass transfer and viscous dissipation over a MHD flow in a vertical porous wall using perturbation method, *International Journal of Heat Mass transfer*, 104 (2017) 409-418.
[3] Rauf, A., Siddiq, M. K., Abbasi, F. M., Meraj, M. A., Asharaf, M., Shehzad, S. A., Influence of convective conditions on three dimensional mixed convection hydromagnetic boundary layer flow of Casson nanofluid, *Journal of Magnetism and Magnetic Materials,* 416 (2016) 200-207.
[4] Hayat, T., Shafiq A., Alsaedi, A., Characteristics of magnetic field and melting heat transfer in stagnation point flow of Tangent- hyperbolic liquid, *Journal of Magnetism and Magnetic Materials*, 405 (2016) 97-106.
[5] Hayat, T., Ullah, I., Muhammad, T., Alsaedi, A., Magnetohydrodynamic (MHD) three-dimensional flow of second grade nanofluid by a convectively heated exponentially stretching surface, *Journal of Molecular Liquids,* 220 (2016) 1004–1012.
[6] Hayat, T., Ullah, I., Farooq, M., Alsaedi, A., Analysis of non-linear radiative stagnation point flow of Carreau fluid with homogeneous-heterogeneous reactions, *Microsystem Technologies,* (2018). https://doi.org/10.1007/s00542-018-4157-y.
[7] Hayat, T., Ullah, I., Ahmad, B., Alsaedi, A., Radiative flow of Carreau liquid in presence of Newtonian heating and chemical reaction, *Results in Physics*, 7 (2017) 715-722.
[8] Hayat T., Ullah, I., Alsaedi, A., Asghar S., Magnetohydrodynamics stagnation-point flow of sisko liquid with melting heat transfer and heat generation/absorption, *Journal of Thermal Science and Engineering Applications*, 10 (2018) 051015.
[9] Hayat, T., Ullah, I., Waqas, M., Alsaedi, A., Flow of chemically reactive magneto Cross nanoliquid with temperature-dependent conductivity, *Applied Nanoscience*, 8 (2018) 1453-1460.
[10] Hayat, T., Ullah, I., Muhammad, T., Alsaedi, A., Radiative three-dimensional flow with Soret and Dufour effects, *International Journal of Mechanical Sciences,* 113 (2017) 829-837.
[11] Hayat, T., Ullah, I., Ahmad, B., Alsaedi, A., MHD mixed convection flow of third grade liquid subject to non-linear thermal radiation and convective condition, *Results in Physics,* 7 (2017) 2804-2811.
[12] Khan, M. I., Waqas, M., Hayat, T., Alsaedi, A., A comparative study of Casson fluid with homogeneous-heterogeneous reactions, *Journal of Colloidal and Interface Science,* 498 (2017) 85-90.
[13] Khan, M. I., Hayat, T., Khan, M. I., Alsaedi, A., Activation energy impact in nonlinear radiative stagnation point flow of Cross nanofluid, *International Communications in Heat and Mass Transfer*, 91 (2018) 216-224.
[14] Hayat, T., Khan, M. I., Qayyum, S., Alsaedi, A., Entropy generation in flow with silver and copper nanoparticles, *Colloids and Surfaces A*, 539 (2018) 335-346.
[15] Hayat, T., Qayyum, S., Khan, M. I., Alsaedi, A., Entropy generation in magnetohydrodynamic radiative flow due to rotating disk in presence of viscous dissipation and Joule heating, *Physics of Fluids,* 30 (2018) 017101.
[16] Hayat, T., Khan, M. I., Qayyum, S., Alsaedi, A., Modern developments about statistical declaration and probable error for skin friction and Nusselt number with copper and silver nanoparticles, *Chinese Journal of Physics*, 55 (2017) 2501-2513.
[17] Hayat, T., Khan, M.I., Qayyum, S., Alsaedi, A., Khan, M. I., New thermodynamics of entropy generation minimization with nonlinear thermal radiation and nanomaterials, *Physics Letters A*, 382 (2018) 749-760.
[18] Hayat, T., Khan, M., Khan, M. I., Alsaedi, A., Ayub, M., Electromagneto squeezing rotational flow of Carbon (Cu)-Water (H2O) kerosene oil nanofluid past a Riga plate: A numerical study, *PLoS ONE*, 12 (8) (2017) e0180976.
[19] Khan, M. I., Ullah, S., Hayat, T., Khan, M. I., Alsaedi, A., Entropy generation minimization (EGM) for convection nanomaterial flow with nonlinear radiative heat flux, *Journal of Molecular Liquids,* 260 (2018) 279-291.
[20] Khan, M. I., Qayyum, S., Hayat, T., Khan, M. I., Alsaedi, A., Khan, T. A., Entropy generation in radiative motion of tangent hyperbolic nanofluid in presence of activation energy and nonlinear mixed convection, *Physics Letters A,* 382 (2018) 2017-2026.
[21] Hossam, S., Hassan, Symmetry Analysis for MHD Viscous Flow and Heat Transfer over a Stretching Sheet, *Applied Mathematics*, 6 (2015) 78-94.
[22] Magyari, E., Keller, B., Heat and mass transfer in the boundary layers on exponentially stretching continuous surface, *Journal of Physics D: Applied Physics*, 32 (1999) 577-585.
[23] Bidin, B., Nazar, R., Numerical solution of the boundary layer flow over an exponentially stretching with thermal radiation, *European Journal of Scientific Research,* 33 (2009) 710-717.
[24] Mukhopadhyay S., Slip effects on MHD boundary layer flows over an exponentially stretching sheet with suction/blowing and thermal radiation, *Ain Shams Engineering Journal*, 4 (2013) 485-491.
[25] Jusoh, R., Nazar, R., Pop, I., Magnetohydrodynamics rotating flow and heat transfer of ferrofluid due to an exponentially permeable stretching/ shrinking sheet, *Magnetism and Magnetic Materials,* 465 (2018) 365-374.



[26] Pal, D., Chatterjee, S., Effects of radiation on Darcy-Forchheimer convective flow over a stretching sheet in a micropolar fluid with non- uniform heat source/sink, *Journal of Applied Fluid Mechanics,* 8(2) (2015) 207-212.
[27] Pal, D., Chatterjee, S., Heat and mass transfer in MHD non-Darcian flow of a micropolar fluid over a stretching sheet embedded in a porous media with non-uniform heat source and thermal radiation, *Communications Nonlinear Science Numerical Simulation*, 15(7) (2010) 1843-1857.
[28] Rahman, M. M., Uddin, M. J., Aziz, A., Effects of variable electric conductivity and non-uniform heat source (or sink) on convective micropolar fluid flow along an inclined flat plate with surface heat flux, *International Journal of Thermal Sciences*, 48(12) (2009) 2331-2340.
[29] Bhukta, D., Dash, G. C., Mishra, S. R., Baag, S., Dissipation effect on MHD mixed convection flow over a stretching sheet through porous medium with non-uniform heat source/sink, *Ain Shams Engineering Journal*, 8 (2017) 353–361.
[30] Mabood, F., Ibrahim, S. M., Effects of Soret and non-uniform heat source on MHD non-Darcian convective flow over a stretching sheet in a dissipative micropolar fluid with radiation, *Journal of Applied Fluid Mechanics,* 9(5) (2016) 2503-2513.
[31] Mabood, F., Ibrahim, S. M., Rashidi, M. M., Shadloo, M. S., Lorenzini, G., Non-uniform heat source/sink and Soret effects on MHD non-Darcian convective flow past a stretching sheet in a micropolar fluid with radiation, *International Journal Heat and Mass Transfer,* 93 (2016) 674–682.
[32] Mahantesh, M., Nandeppanavar, K., Vajravelu, M., Abel, S., Heat transfer in MHD viscoelastic boundary layer flow over a stretching sheet with thermal radiation and non-uniform heat source/sink, *Communications Nonlinear Science Numerical Simulation*, 16 (2011) 3578–3590.
[33] Ramesh, G. K., Chamkha, A. J., Gireesha, B. J., MHD mixed convection flow of a viscoelastic fluid over an inclined surface with a non-uniform heat source/sink, *Canadian Journal of Physics*, 91(12) (2015) 1074-1080.
[34] Ramesh, G. K., Gireesha, B. J., Bagewadi, C. S., MHD flow of a dusty fluid near the stagnation point over a permeable stretching sheet with non-uniform source/sink, *International Journal Heat and Mass Transfer,* 55 (2012) 4900–4907.
[35] Sandeep, N., Sulochana, C., Dual solutions for unsteady mixed convection flow of MHD micropolar fluid over a stretching/shrinking sheet with non-uniform heat source/sink, *Engineering Science and Technology,* doi.org/10.1016/j.jestch.2015.05.006.
[36] Chamkha, A.J., MHD flow of a uniformly stretched vertical permeable surface in the presence of heat generation/absorption and a chemical reaction, *International Communications in Heat and Mass Transfer*, 30(3) (2003) 413–422.
[37] Patil, P. M., Pop, I., Effects of surface mass transfer on unsteady mixed convection flow over a vertical cone with chemical reaction, *Heat and Mass Transfer*, 47 (2011) 1453-1464.
[38] Patil, P. M., Shashikant, A., Roy, S., Momoniat E., Unsteady mixed convection over an exponentially decreasing external flow velocity, *International Journal of Heat and Mass Transfer*, 111 (2017) 643-650.
[39] Patil, P. M., Chamkha, A. J., Roy, S., Effects of chemical reaction on mixed convection flow of a polar fluid through a porous medium in the presence of internal heat generation, *Meccanica*, 47 (2012) 483-499.
[40] Patil, P. M., Roy, S., Pop, I., Chemical reaction effects on unsteady mixed convection boundary layer flow past a permeable slender vertical cylinder due to a nonlinearly stretching velocity, *Chemical Engineering Communications*, 200 (2013) 398-417.
[41] Schlichting, H., Gersten, K., *Boundary Layer Theory*, Springer, New York, 2000.
[42] Patil, P. M., Ramane, H. S., Roy, S., Hindasageri, V., Momoniat, E., Influence of mixed convection in an exponentially decreasing external flow velocity, *International Journal of Heat and Mass Transfer*, 104 (2017) 392-399.
[43] Patil, P. M., Latha, D. N., Roy, S., Momoniat, E., Double diffusive mixed convection flow from a vertical exponentially stretching surface in presence of the viscous dissipation, *International Journal of Heat and Mass Transfer*, 112 (2017) 758-766.
[44] Varga, R.S., *Matrix Iterative Analysis*, Prentice-Hall, USA, 2000.

## ORCID iD

A.J. Chamkha https://www.orcid.org/0000-0002-8335-3121